Aerodynamic Shape Optimization Using the Discrete Adjoint of the Navier-Stokes Equations: Applications towards Complex 3D Configurations

Joël Brezillon, Richard P. Dwight[†]
German Aerospace Center (DLR), Institute of Aerodynamics and Flow Technology,
Lilienthalplatz 7, 38108 Braunschweig, Germany, Joel.Brezillon@dlr.de

Abstract

Within the next few years, numerical shape optimization based on high fidelity methods is likely to play a strategic role in future aircraft design. In this context, suitable tools have to be developed for solving aerodynamic shape optimization problems, and the adjoint approach - which allows fast and accurate evaluations of the gradients with respect to the design parameters - is seen as a promising strategy. After describing the theory of the viscous discrete adjoint method and its implementation within the unstructured RANS solver TAU, this paper describes application for aerodynamic shape optimization. First wing and fuselage designs of the DLR-F6 wing-body aircraft are presented. A step forward in complexity is considered by applying the adjoint for flap and slat optimal settings of the DLR-F11 model, a wing-body aircraft in high-lift configuration. On all cases presented, optimization were successfully performed within a limited number of flows evaluations.

1 Introduction

Numerical shape optimization is playing an increasing strategic role in aerodynamic aircraft design. It offers the possibility of designing or improving aircraft components with respect to a given objective, subject to geometrical and physical constraints. However Computational Fluid Dynamics (CFD) still suffers from high computational effort for flow simulations around realistic 3d configurations which limits its use in design process. Consequently, worldwide a large effort is being devoted to developing efficient optimization strategies for industrial aerodynamic aircraft design.

At the DLR, activities focus on developing several key technologies relating to the establishment of an efficient and flexible numerical optimization capability based on high fidelity methods. These include suitable techniques for geometry parameterization, meshing and mesh movement methods, efficiency and accuracy improvements of the flow solvers, as well as robust and efficient optimizers. One of the most promising strategies is the use of the adjoint approach [1,2,3,4] of a flow solver for efficient and accurate computation of gradients in high-dimensional design spaces, which can then be applied within, among other, gradient-based optimizers.
The paper will give an overview of the work performed at the German Aerospace Center's Institute of Aerodynamics and Flow Technology, on the application of the discrete adjoint approach for solving various aerodynamic shape optimization problems. The paper introduces first the strategy developed in the unstructured *TAU* code [5,6,7] to solve the adjoint problem and to compute the gradients. In the second part, the paper focuses on the application to 3d design in cruise and take-off conditions.

2 Gradients via adjoint approach

2.1 Primal approach

Let the optimization problem be stated as

$$\min_{w.r.t.\ D} I(W, X, D), \tag{1}$$

subject to the constraint

$$R(W, X, D) = 0, \tag{2}$$

where I is a cost function such as lift or drag, D is a vector of design variables that can include the angle of incidence and control shape of aircraft subject to aerodynamic design, $W(X,D)$ the vector of flow variables, $X(D)$ the computational mesh and $R(W,X,D)$ the residuals of the flow.
For a gradient based optimization strategy, the search for the minimum requires the total derivative of the cost function I with respect to the design variables D. This total derivative - also called here the sensitivity - can be written as:

[†] Now in Aerodynamics Group, Aerospace Faculty, TU Delft <r.p.dwight@tudelft.nl>

$$\frac{dI}{dD} = \frac{\partial I}{\partial D} + \frac{\partial I}{\partial X}\frac{dX}{dD} + \frac{\partial I}{\partial W}\frac{dW}{dD}. \tag{3}$$

The two first terms of (3) expresses the direct effect of design parameter and of the geometry perturbation on the cost function *I* respectively and the last term contains the effect of the flow alteration caused by the geometry perturbation. Solving the above equation can be done by applying finite differences which requires evaluations of the flow solver on *n* perturbed geometries, with *n* the number of design parameter. Alternatively, the adjoint approach allows a rapid evaluation of *dI/dD* for a large number of design variables *D*, without computing the flow solution on the perturbed geometry.

2.2 Dual approach

Instead of applying the chain rule to *I*, apply it to the Lagrangian:

$$L(W, X, D, \Lambda) = I(W, X, D) + \Lambda^T R(W, X, D) \tag{4}$$

where Λ are known as the adjoint variables. Since (2) holds for all *D*, *L=I* for all Λ and all *D*. Hence,

$$\frac{dL}{dD} = \frac{dI}{dD} \qquad \forall \Lambda, D. \tag{5}$$

and so, applying the chain rule to *L*, the total derivative of *I* becomes:

$$\begin{aligned} \frac{dL}{dD} &= \left\{\frac{\partial I}{\partial D} + \frac{\partial I}{\partial X}\frac{dX}{dD} + \frac{\partial I}{\partial W}\frac{dW}{dD}\right\} + \Lambda^T\left\{\frac{\partial R}{\partial D} + \frac{\partial R}{\partial X}\frac{dX}{dD} + \frac{\partial R}{\partial W}\frac{dW}{dD}\right\}, \\ &= \left\{\frac{\partial I}{\partial D} + \Lambda^T\frac{\partial R}{\partial D}\right\} + \left\{\frac{\partial I}{\partial X} + \Lambda^T\frac{\partial R}{\partial X}\right\}\frac{dX}{dD} + \left\{\frac{\partial I}{\partial W} + \Lambda^T\frac{\partial R}{\partial W}\right\}\frac{dW}{dD}. \end{aligned} \tag{6}$$

The unknown quantity *dW/dD* may be eliminated by choosing Λ such that

$$\left(\frac{\partial R}{\partial W}\right)^T \Lambda = -\left(\frac{\partial I}{\partial W}\right)^T. \tag{7}$$

This is the adjoint equation, and must be solved only once to evaluate the gradient of a single *I* with respect to any number of design variables. The resulting Λ allows rapidly computing the total derivative using:

$$\frac{dI}{dD} = \left\{\frac{\partial I}{\partial D} + \Lambda^T\frac{\partial R}{\partial D}\right\} + \left\{\frac{\partial I}{\partial X} + \Lambda^T\frac{\partial R}{\partial X}\right\}\frac{dX}{dD}. \tag{8}$$

2.3 Implementation of the discrete adjoint approach

The discrete variant of the adjoint equation (7) is now considered. Its implementation requires the ability to evaluate the quantities $\Lambda^T\left(\partial R / \partial W\right)$ - the adjoint residual – and $\partial I / \partial W$.
The Jacobian $\left(\partial R / \partial W\right)$ is evaluated by hand, which is a straightforward exercise as *R* may be written explicitly in terms of *W*, while being time-consuming as *R* is often extremely complex. As *R* is a sum of convective fluxes, viscous fluxes, boundary conditions etc., each of these may be handled independently, and by application of the chain rule may be further subdivided into manageable chunks. The derivatives are further simplified by choosing primitive variables as working variables. Because the equations remain in conservative form this choice has no effect on the final solution. A more detailed description of the implementation in the TAU code can be found in [8]. A wide range of the spatial discretizations available in TAU have been differentiated, including the Spalart-Allmaras-Edwards one-equation turbulence model. The effect of various approximations of the Jacobian was investigated and their impacts on the efficiency of the optimization process has been demonstrated on several 2d optimization problems [8,9]. In the present study, the viscous 3d adjoint computations have been performed by freezing turbulent quantities – i.e. assuming they are invariant with respect to the linearization. This is necessary because incorporating the linearization of the turbulence equations resulting in an exceptionally poorly conditioned Jacobian matrix, which is not amenable to solution with conventional iterative methods.

Despite the guarantees regarding convergence provided by the theory of adjointed fixed-point iterations (FPIs) [10] there are regularly situations in which it is possible to obtain a reasonably converged solution of the non-linear equations, but not of the corresponding adjoint equations. This can occur for three reasons: either a) the non-linear

solution is not sufficiently converged, or b) there is a discrepancy between the linear and non-linear problem due to some approximation of the Jacobian, or c) the FPI applied to the non-linear problem does not converge *asymptotically* itself. All three cases appear regularly in practice. An engineer may reasonably consider a computation converged when the integrated forces that interest her no longer vary significantly, though this may occur prior to the asymptotic regime.

In an effort to understand and mitigate these phenomena, we consider the Recursive Projection Method (RPM), originally developed by Schroff and Keller in 1993 as a means of stabilizing unstable procedures [11]. The main idea can be described briefly as follows: let the (linear) adjoint system be written $Ax=b$, and regard the transient solution of the linear problem as a sum of eigenvectors of the relaxation operator $\Phi = (I - M^{-1}A)$ where M is some iteration operator, e.g. LU-SGS with multigrid. The application of Φ to an approximate solution then corresponds to a product of each eigenvector with its corresponding eigenvalue. Divergence of the iteration implies that there is at least one eigenvalue of Φ with modulus greater than unity. Assuming that the number of such eigenvalues is small, and that the space spanned by their eigenvectors is known, call it P, then it must be possible to solve the projection of the problem onto this low dimensional subspace using some expensive but stable method, while solving the projection onto the complimentary subspace Q using the original FPI iteration, which is known to be stable there.

Newton-Raphson is therefore used on P. The space of dominant eigenvectors is determined as the calculation progresses, by applying the principle that the difference between successive applications of the FPI on Q form a power iteration on the dominant eigenvalues of Φ restricted to Q.

This procedure has been successfully applied for the design of DLR-F6 configuration that features flow separation in the junction between the upper surface of the wing and the fuselage, see Section 3.

Further investigations revealed that the robustness of RPM for the viscous adjoint problem was limited in the case that the base iteration diverges too rapidly for P to be well approximated. In this case applying the well-known Generalized Minimum Residual (GMRes) method in it's restarted form [12], with 10-50 iterations of LU-SGS with multigrid as a preconditioner has been seen to be an exceptionally robust alternative (although still not robust enough to solve systems including full turbulence model linearization in general). This was the stabilization using to converge the adjoint problem for the high-lift configuration in Section 4.

2.4 The metric terms

In order to compute the total derivatives of the cost function I as given in (8), the metric term variation is computed by using finite differences, which is in case of R computed like:

$$\frac{\partial R}{\partial X}\frac{dX}{dD_k} \approx \frac{R(W, X(D+\Delta D_k) - R(W, X)}{\Delta D_k} = \frac{\Delta R}{\Delta D_k}. \tag{9}$$

After obtaining Λ, the sensitivities can be evaluated with a single point deformation and yields for each design variable D_k to a variation of the cost function due to the perturbed geometry and we get a scalar difference for the direct variation and a matrix-vector product for the dependency of the residual,

$$\frac{dI}{dD_k} \approx \frac{\Delta I}{\Delta D_k} + \Lambda^T \frac{\Delta R}{\Delta D_k}. \tag{10}$$

3 Shape optimizations of the DLR-F6 configuration

The adjoint method is first applied to the drag minimization of the DLR-F6 wing-body configuration at Mach 0.75, a Reynolds number of 3×10^6, and lift coefficient 0.5, at which conditions the case has a large region of separated flow in the junction between the upper surface of the wing and the fuselage, as well as along most of the length of the wing. Here, the discrete variant of adjoint formulation is used and the standard method of adjointed LU-SGS with multigrid alone was unconditionally unstable, and applying RPM was necessary to obtain a converged solution.
The optimization algorithm used is conjugate-gradients (CG), as in [13], where the angle-of-attack is automatically set by TAU to maintain constant lift. The computational grid - shown in FIG. 1 - is coarse but sufficient to resolve the separation mentioned.

The geometry is parametrized by the coordinates of the lattice box points controlling the free-form deformation (FFD) [14,15,16,17]. The FFD technique allows a broad range of deformations with a low number of parameters and ensures a smooth deformation. The lattice boxes were generated with DLR's parametric grid generator MegaCads [18].

3.1 Wing shape optimization

For the wing optimization, the vertical positions of 84 paired nodes of the free-form deformation bounding box as well as 12 additional wing twist variables are used as design parameters, see FIG. 2. In total the wing is parametrized with 96 variables and the pairing of nodes ensures that the wing thickness remains unchanged during the optimization. With such a large number of design variables only gradient-based optimization is viable, and only the adjoint method can deliver the gradient efficiently. Note that since the bounding box passes inside the fuselage, the wing-body junction also varies, and this is accounted for by the geometry and grid generation process. The metric sensitivities needed in the gradient calculation are evaluated by finite-differences using mesh deformation.
The convergence of the optimization is shown in FIG. 3, the horizontal axis shows the number of calls to the flow solver (both linear and non-linear), thereby approximately representing computational effort. Symbols indicate gradient evaluations. After 32 solver calls CG was unable to reduce the drag further, giving a final reduction of about 10 drag counts (1 drag count equal to 0.0001). In contrast a similar optimization with 42 parameters produced a reduction of only 8 counts on this mesh (in a similar CPU time) [13], emphasizing the need for a comprehensive parameterization. The optimization reduced the region of corner separation considerably, FIG. 4, while not completely eliminating it, which is unlikely to be possible within the design space considered, as it does not allow deformation of the fuselage.

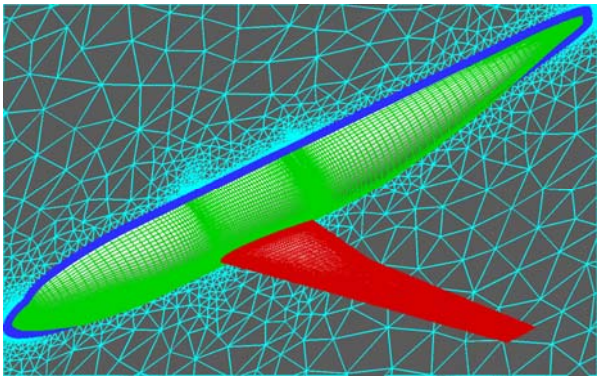

FIG. 1. Mixed structured/unstructured Navier-Stokes meshes of the DLR-F6 configuration.

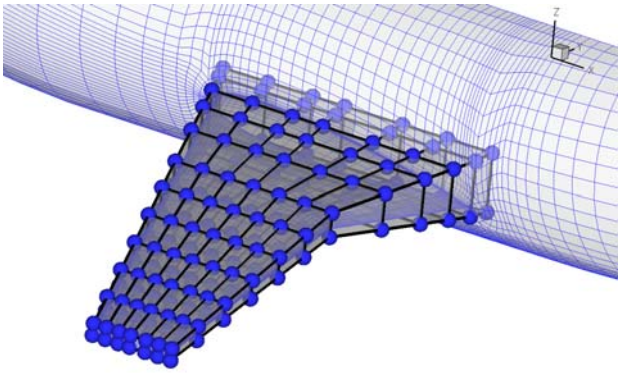

FIG. 2. Parameterization of the wing with a free-form deformation box with 84 paired nodes. Twist is parameterized separately with 12 variables.

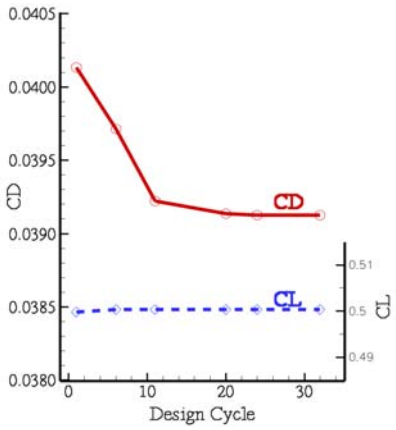

FIG. 3. Convergence of the DLR-F6 wing shape drag-minimization optimization.

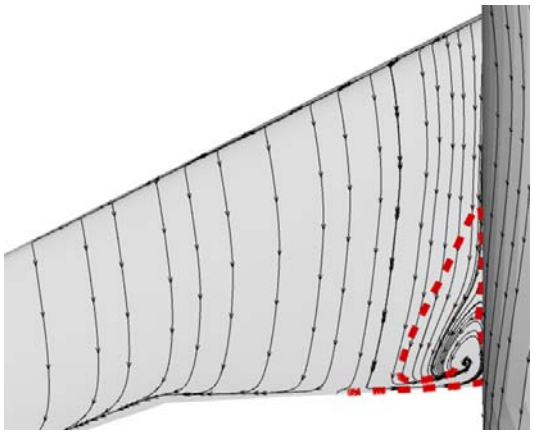

FIG. 4. Comparison of the region of corner separation before (presented with the dashed line) and after wing shape optimization.

3.2 Fuselage shape optimization

As second demonstration, the fuselage shape is now optimized by considering the wing shape constant. This exercise intends to demonstrate the possibility of removing the flow separation by shaping the fuselage. Here also, the free-form deformation is employed and a representation of the bounding box around the fuselage is given in FIG. 5. The horizontal displacements of 25 nodes, concentrated around the intersection line, are selected as design variables. The node displacement is not restricted to any direction and can lead to an increase or a decrease of the volume of the fuselage. After deformation, the intersection line is recomputed with the in-house tool MegaCads.
After 46 flow evaluations and 7 gradient evaluations, the optimization process converges to a final configuration by keeping constant the lift coefficient, see FIG. 6. The new optimized configuration has almost 20 drag counts less than the baseline configuration. This drag improvement is 2 times higher than observed on the previous optimization.
FIG. 7 shows a comparison of the region of corner separation before and after optimization of fuselage shape. In fact the optimization procedure was able to completely remove the flow separation. Close to the trailing edge of the wing, the new fuselage presents a shape similar to a fairing as observed on modern aircraft. A side view of the optimised wing-body intersection shows a more complex 3d shape, with parts going into the fuselage, FIG. 8. The optimization process perfectly adapts the shape to the flow in order to avoid separation. This result demonstrates the accuracy of the adjoint approach for computing gradients and the flexibility of the optimization process to handle complex 3d aerodynamic flows.

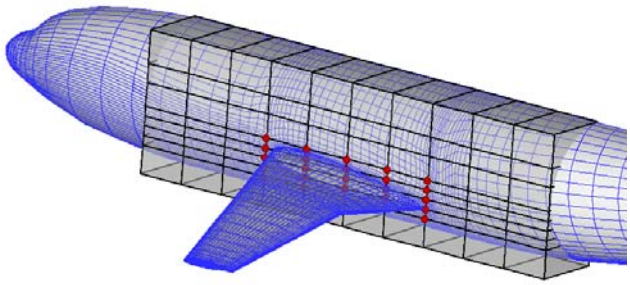

FIG. 5. Parameterization of the fuselage with a free-form deformation box with 25 active nodes (red spheres).

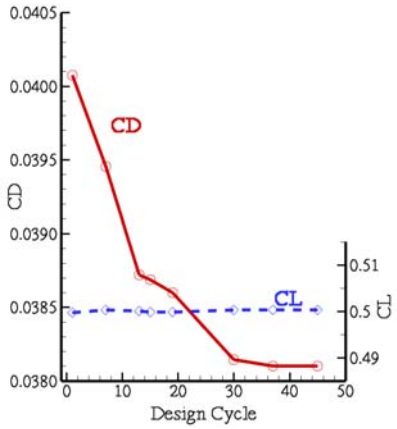

FIG. 6. Convergence of the DLR-F6 fuselage drag-minimization optimization.

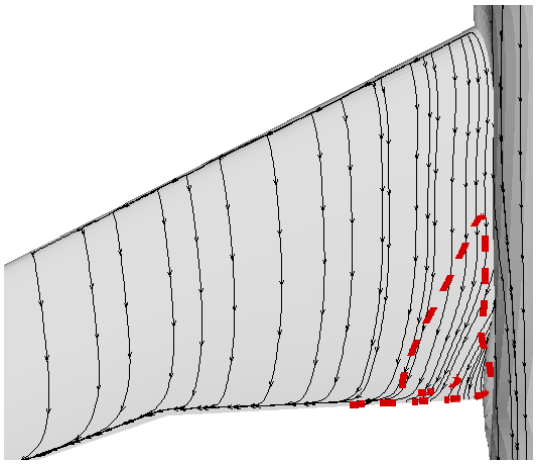

FIG. 7. Comparison of the region of corner separation before and after fuselage shape optimization (dashed line represents the limit of flow separation on baseline configuration).

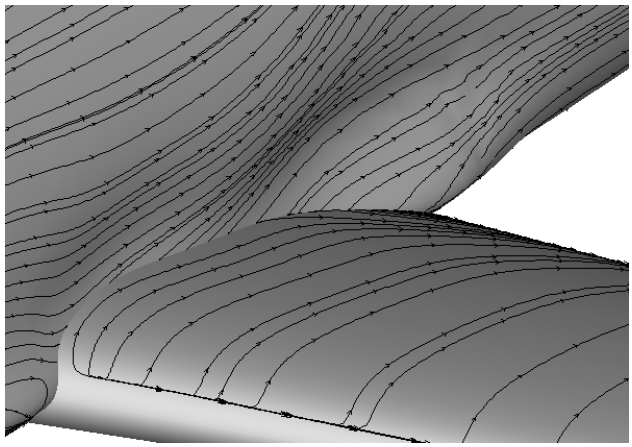

FIG. 8. Close view of the wing-body intersection after optimization of the fuselage shape.

4 Flap and slat settings optimization of the DLR-F11 aircraft

The last configuration optimized is the so called DLR-F11 model with full span flap and slat in take-off configuration, see FIG. 9. This model is a wide-body Airbus-type research configuration with a half span of 1.4 meter that can feature different degrees of complexity [19]. Here six design variables are selected to modify the deflections, the horizontal and the vertical positions of the flap and the slat. The geometric changes are propagated homogeneously along the span. The goal is to maximize at a single take-off condition (Mach=0.3; Re=20x10^6; AoA=8^o) a derived expression of the lift to drag ratio:

$$\text{Obj} = \frac{C_L{}^3}{C_D{}^2}. \qquad (11)$$

This performance indicator, based on the climb index, has already been successfully employed for flap design based on 2d computations and turned to be better suited than the lift to drag ratio [20]. Additionally, the lift is not allowed to decrease and the angle of attack is kept fixed. In order to make a more realistic optimization the weight of the high-lift system kinematics, which depends on the horizontal deployment capability, is taken into account by penalizing the objective function to avoid too heavy a mechanism. The relation between the horizontal displacement and the penalty is set according to industrial specifications [20].

An ICEM-CFD macro has been developed to handle both the parameterization and the mesh procedure. This macro first sets the position of the elements according to the design variables and computes automatically the flap and slat intersection lines with the body. Once the CAD geometry is ready, the meshing part starts and automatically projects the mesh on the moving part and on the updated intersections lines, sets the position and size of the O blocks surrounding the elements. The resulting mesh has in total 2.5 millions points, see FIG. 9. The complete process, from reading the design variables to writing the mesh in unstructured formats takes about 1 minute on a single AMD Opteron 2.5 GHz processor.

The numerical simulations are based on the RANS equations and the Spalart-Allmaras-Edwards turbulence model. For fast convergence, the low Mach number preconditioning approach is adopted and the steady state is reached by a Runge-Kutta scheme using multigrid W-cycles on 3 levels. A fully converged solution with almost 5 orders of density residual decrease is obtained after 5,000 TAU cycles.
In order to exploit the parallel capability of the TAU code, the aerodynamic flow is computed on a cluster of 32 AMD Opteron 2.4 GHz processors and the drag and lift adjoints are computed simultaneously on 2 clusters of 16 processors each. Each solution is fully converged after 3 hours wall clock time.

FIG. 10 presents the evolution of the optimization process obtained with the NLPQLP optimization strategy [21] available in modeFRONTIER [22] coupled to the adjoint approach for the computations of the gradients. After 13 evaluations and 78 hours of simulations the optimization converged to a maximum with a limited deviation on the lift coefficient. The performance improvement is made evident by plotting the drag distribution in span-wise direction for each element, see FIG. 11 and FIG. 12: the optimization has almost no influence on the lift and drag of the body and the flap but permits to made further negative the drag on the slat by increasing the lift. This improvement has to be paid by a drag increase and lift loss on the main wing. Finally, the optimized configuration has in total 17.8 counts less drag than on the baseline configuration by same lift coefficient.

Thanks to the adjoint approach, the process is almost independent of the number of design variables and a more complex optimization problem involving more design parameters should require almost the same turn around time.

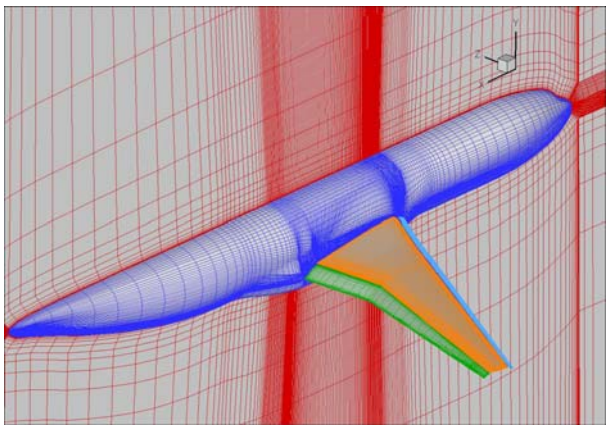

FIG. 9. Mesh around the DLR-F11 model in full span flap and slat configuration.

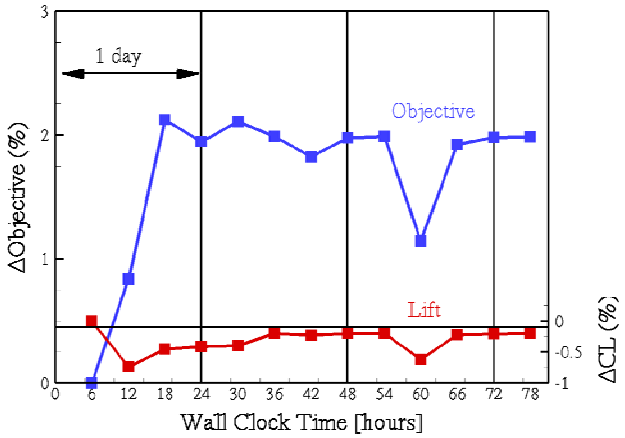

FIG. 10. Evolution of the objective and lift coefficient according to the wall-clock time.

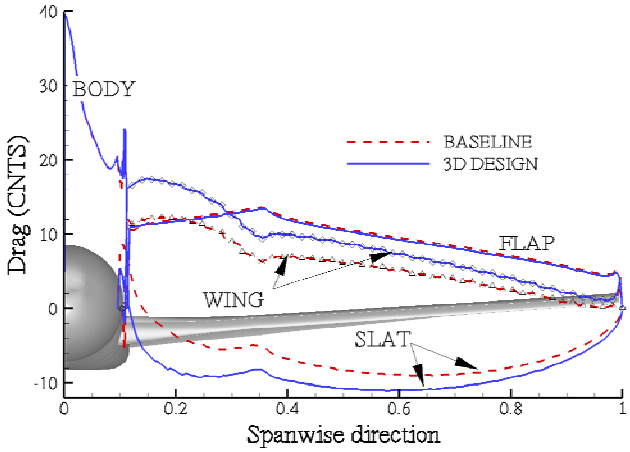

FIG. 11. Drag distribution along the spanwise direction on the baseline and optimised configurations.

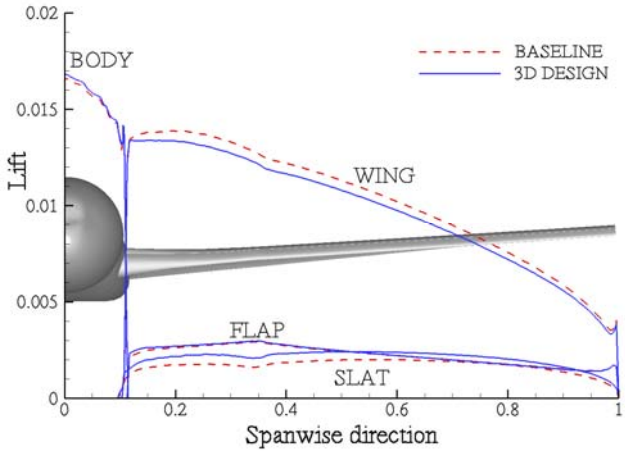

FIG. 12. Lift distribution along the spanwise direction on the baseline and optimised configurations.

Conclusion

This article presented activities carried out at the DLR for the development of the discrete adjoint approaches in the unstructured RANS solver TAU code and its application to solving wide range of aerodynamic shape designs.

The capability of the adjoint approach to handle problems with large number of design parameters has been first demonstrated for the optimization of the DLR-F6 configuration in viscous flow. It has been observed that the region of separation was considerably reduced thanks to the fine parameterization of the wing. When the fuselage is parametrized, the optimization process is able to remove the flow separation within a limited number of flow computations. It can be pointed out that the free form deformation is here a key technology for the parametrization of critical area.

These successful optimizations confirm the accuracy of the developed adjoint based procedure for computing the gradients.

The method has been then applied to perform the settings optimizations of 3d high-lift configurations. Thanks to the adjoint approach, only a few flow computations were required to converge the optimization problem. The inclusion of the adjoint approach gives new opportunities to treat more complex optimization problems in limited turn around time.

Near future activities will focus on improvement of the evaluation of the metric terms in order to compute more efficiently the gradients. From the applications point of view, future work will deal with multi-points problems for robust design and on other complex configurations, such as engine integration problems.

Acknowledgement

The work presented here was part of the MEGADESIGN project, financed by the German Government in the framework of the aeronautical research program. This funding is here gratefully acknowledged.

References

[1] Jameson A (1988) Aerodynamic design via control theory. Journal of Scientific Computing 3 (3), pp. 233-260

[2] Jameson, A (1995) Optimum aerodynamic design using CFD and control theory AIAA 95-1729, in: AIAA 12th Computational Fluid Dynamics Conference, San Diego.

[3] Anderson, W. K. and Venkatakrishnan, V. (1997) Aerodynamic Design Optimization on Unstructured Grids with a Continuous Formulation. AIAA Paper 97-0643.

[4] Giles, M.; Pierce, N. (1999) An introduction to the adjoint approach to design. Proceedings of ERCOFTAC Workshop on Adjoint Methods.

[5] Galle, M.(1999) Ein Verfahren zur numerischen Simulation kompressibler, reibungsbehafteter Strömungen auf hybriden Netzen. DLR-FB 99-04.

[6] Gerhold, Th. (2005) Overview of the Hybrid RANS TAU-Code In: Kroll, N., Fassbender, J. (Eds) MEGAFLOW Numerical Flow Simulation Tool for Transport Aircraft Design, Notes on Multidisciplinary Design, Vol. 89, Springer.

[7] Schwamborn, D., Gerhold, T., Heinrich, R. (2006) The DLR TAU-Code: Recent Applications in Research and Industry. Proceedings of ECCOMAS CFD 2006, Delft The Netherland.

[8] Dwight, R. (2006) Efficiency Improvements of RANS-Based Analysis and Optimization using Implicit and Adjoint Methods on Unstructured Grids. School of Mathematics, University of Manchester

[9] Dwight, R.; Brezillon, J. (2006) Effect of Various Approximations of the Discrete Adjoint on Gradient-Based Optimization. Proceedings of the 44th AIAA Aerospace Sciences Meeting and Exhibit, AIAA Paper 2006-0690, Reno NV.

[10] Dwight, R.; Brezillon, J.; Vollmer, D.B. (2006): Efficient Algorithms for Solution of the Adjoint Compressible Navier-Stokes Equations with Applications. Proceedings of the ONERA-DLR Aerospace Symposium (ODAS), Toulouse.

[11] Schroff, G.; Keller, H. (1993) Stabilization of unstable procedures: The Recursive Projection Method. SIAM Journal of Numerical Analysis 30, 10991120

[12] Saad Y.; Schultz MH (1988) A generalized minimum residual algorithm for solving non-symmetric linear systems. SIAM Journal of Scientific and Statistical Computing, Vol. 7, No. 3, pp. 856-859.

[13] Brezillon, J., Brodersen, O., Dwight, R., Ronzheimer, A., Wild, J. (2006) Development and application of a flexible and efficient environment for aerodynamic shape optimisation. In: Proceedings of the ONERA-DLR Aerospace Symposium (ODAS), Toulouse.

[14] Samareh, J.A.(1999) Novel Shape Parameterization Approach. NASA TM-1999-209116

[15] Samareh, J.A. (2004) Aerodynamic Shape Optimization Based on Free-Form Deformation. AIAA 2004-4630

[16] Ronzheimer, A. Post-Parametrisation of CAD-Geometries Using Freeform Deformation and Grid generation Techniques. Notes on Numerical Fluid Mechanics and multidisciplinary Design, Vol. 87, pp. 382-389

[17] Ronzheimer, A. (2005) Shape Parameterization in Multidisciplinary Design Optimization Based on Freeform Deformation. Evolutionary and Deterministic Methods for Design, Eurogen, Munich

[18] Brodersen, O.; Hepperle, H.; Ronzheimer, A.; Rossow, C.-C.; Schöning, B. (1996) The Parametric Grid Generation System Mega Cads. 5th International Conference on Numerical Grid Generation in Computational Field Simulation, national Science Foundation.

[19] Rudnik R., Thiede P.(2005) European research on high lift commercial aircraft configurations in the EUROLIFT projects. CEAS/KATnet Conference on Key Aerodynamic Technologies, Bremen, DE.

[20] Wild J, et al..(2007) Advanced high-lift design by numerical methods and wind tunnel verification within the European project EUROLIFT II. 25th Applied Aerodynamics Conference, AIAA-2007-4300, Miami, USA.

[21] Schittkowski K. (2001) NLPQLP: A new Fortran implementation of a sequential quadratic programming algorithm for parallel computing. Report, Department of Mathematics, University of Bayreuth.

[22] Esteco, modeFRONTIER v4, http://www.esteco.com/